### Title

A new satellite-based global climatology of dust aerosol optical depth A new satellite-based global climatology of dust aerosol optical depth




### Journal

Journal of Applied Meteorology and Climatology, 59(1)

### ISSN

1558-8424



### Authors

Voss, Kara K
Evan, Amato T



### Publication Date

2020

### DOI

10.1175/jamc-d-19-0194.1

Peer reviewed

JOURNAL OF APPLIED METEOROLOGY AND CLIMATOLOGY

# A new satellite-based global climatology of dust aerosol optical depth

KARA K. VOSS* AND AMATO T. EVAN†

*Scripps Institution of Oceanography, University of California San Diego, La Jolla, CA*

ABSTRACT

Dust is the largest contributor to global aerosol loading, by mass. Yet, long term observational records of dust, particularly over the ocean, are extremely limited. Here, two nearly-global observational datasets of dust aerosol optical depth ($\tau_{du}$) are created based primarily on optical measurements of the aerosol column from 1) the MODerate resolution Imaging Spectroradiometer (MODIS) aboard the Terra satellite spanning from 2001 to 2017 and 2) the Advanced Very High-Resolution Radiometer (AVHRR) from 1981 to 2017. The quality of the new data is assessed by comparison with other high-quality but less comprehensive measurements. Retrievals of aerosol optical thickness from AVHRR are limited where there is optically thick dust, causing a substantial negative bias in the seasonal mean $\tau_{du}$ over characteristically dusty regions. The climatology of $\tau_{du}$ based on MODIS retrievals compares well with two in-situ measurements of dust. Between 2001 and 2017, $\tau_{du}$ decreased over Asia and increased significantly over the Sahara, Middle East, and parts of eastern Europe, with the largest increase found over the Aral Sea where emissive playa surfaces are exposed. Between 1981 and 2017, $\tau_{du}$ increased near the Arabian Peninsula and decreased in the tropical North Atlantic near Cape Verde. These daily, observational and quasi-global records of dust allow for a deepening of our understanding of the impacts of dust on climate and may prove useful for evaluating its representation in climate models.

## 1. Introduction

Aeolian dust makes up the largest mass fraction of the global aerosol burden, and produces profound impacts on the natural and anthropological system (Textor et al. 2006). Dust becomes aerosolized when windblown sand saltates, ejecting mineral particles from the disturbed soil that are small enough to remain in the air (Gillette et al. 1974; Shao et al. 1993). These particles can then have impacts locally, or can impact areas far from their source by remaining lofted for weeks at a time to be transported thousands of miles in the prevailing winds (Prospero 1999; Duce et al. 1980; Uematsu et al. 1983). Through direct radiative effects, aeolian dust it is known to impact sea surface temperature and precipitation patterns (Yoshioka et al. 2007; Evan et al. 2009; Foltz and McPhaden 2008). Through indirect effects, when acting as cloud or ice nuclei, dust is known to impact cloud microphysics, cloud persistence (Rosenfeld et al. 2001; Kaufman et al. 2005), and precipitation (Isono et al. 1959; DeMott et al. 2003; Ault et al. 2011; Creamean et al. 2013, 2016; Fan et al. 2014). In the tropical North Atlantic, it is known to shape the development of some tropical cyclones, at times controlling both spatial structure and intensity (Evan et al. 2006; Dunion and Velden 2004; Lynn et al. 2016). Additionally, dust impacts the human system in ways that can be detrimental to human health (Tong et al. 2017; Griffin 2007), agricultural systems (Brown 2002), and transportation (Shao 2008; Mani and Pillai 2010; Ai and Polenske 2008),

Climate models underestimate dust aerosol optical depth and dust emission from Africa, limiting their ability to provide meaningful insight into its impacts on future climate (Evan et al. 2014), and projected trends in dust aerosol emission are spatially heterogeneous and highly uncertain (Pu and Ginoux 2017; Mahowald and Luo 2003; Tegen et al. 2004). A major limiting factor in understanding the global distribution of dust, how it will change in the future, and its complex impacts, is the limited availability of measurements, especially over the ocean (Prospero and Mayol-Bracero 2013). Airborne campaigns have provided measurements for select places and times (Ralph et al. 2016; Formenti 2003; Chen et al. 2011; Formenti et al. 2008; Stith et al. 2009; Ryder et al. 2013; Klaver et al. 2011), and ground based networks have provided long term measurements for specific regions (Malm et al. 1994; Prospero and Nees 1986; Prospero 1999; Holben et al. 1998).

Several studies have used satellite-based products to study dust aerosol optical depth (DAOD) over either

*Corresponding author address: Scripps Institution of Oceanography, University of California San Diego, 9500 Gilman Dr., La Jolla, CA

E-mail: kvoss@ucsd.edu

†Scripps Institution of Oceanography, University of California San Diego, 9500 Gilman Dr., La Jolla, CA

the ocean or land in select locations. Over the Atlantic Ocean, Kaufman (2005) analyzed dust aerosol optical depth ($\tau_{du}$) using the MODerate Imaging Spectroradiometer (MODIS) retrievals of aerosol optical depth (AOD), and Evan and Mukhopadhyay (2010) used a similar method to create a record of DAOD based on retrievals by the Advanced Very High Resolution Radiometer (AVHRR). Ginoux et al. (2012) used $\tau_{du}$ over bright land surfaces based on MODIS Deep Blue AOD to identify dust source regions, and Ridley et al. (2016) produced a long-term mean dataset of DAOD between 2004 and 2008 using AOD retrievals from multiple satellite platforms and dust estimates from several global models.

Here, we expand on the work of Evan and Mukhopadhyay (2010) by using the extended record of satellite retrievals to produce two nearly-global $\tau_{du}$ datasets developed using MODIS (2001-2017) and AVHRR (1981-2017) with the former dataset extended to cover both land and ocean regions. The first dataset, extending from 2001 to 2017, is produced over land and water surfaces at 1° x 1° resolution and compares well with independent measurements of dust in the western U.S. and in the Carribean. These $\tau_{du}$ estimates elucidate increasing dust trends in the Sahara and parts of the U.S. and decreasing trends in Asia for the temporal limits of the record. The second dataset extends from 1981 to 2017 at the same spatial resolution as the first dataset.

In the next section, we describe the data and methods used in the estimation of global $\tau_{du}$, and a an estimation of the associated uncertainty. Our results, in Section 3, include identification of climatological seasonal patterns in $\tau_{du}$, a comparison our $\tau_{du}$ estimates as derived from two different sensors, and a comparison of the the preferred dataset to pre-existing ground based measurements of dust aerosol from several locations. We then identify regional trends in dust aerosol optical depth for the period of each record.

## 2. Methodology

Two datasets of $\tau_{du}$ were created. This first, which hereafter will be referred to as $\tau_{du,MODIS}$, is based primarily on AOD retrievals from the MODIS instrument on the Terra platform, with a companion set of estimates created for the same instrument aboard the Aqua platform, (both accessed at https://ladsweb.modaps.eosdis.nasa.gov) and extends from 2001 through 2017. The $\tau_{du,MODIS}$ dataset includes estimates over both land and water-covered surface. The second dataset, which combines aerosol optical thickness (AOT) retrievals from the AVHRR instruments aboard the NOAA series of satellites over the period 1981 through 2017, will be called $\tau_{du,AVHRR}$ (Heidinger et al. 2014; Zhao et al. 2008, 2002; Zhao and Program 2017). $\tau_{du,AVHRR}$ estimates are only provided over water as AVHRR AOT retrievals are not available over land.

### *a. Datasets used*

MODIS level 3, collection 6 daily AOD is derived from the measured 500 m resolution radiance from all visible MODIS bands by taking the average of the measured radiance over all scenes that are cloud-free and glint-free over the ocean within a 10km grid box, and fitting these values to a lookup table. MODIS fine mode fraction (FMF) is a ratio of the small mode AOD to the total AOD. MODIS AOD over ocean has been shown to have an expected error of $\Delta\tau \pm 0.03 \pm 0.05\tau$ (Kaufman et al. 1997; Tanré et al. 1997). For dust dominated regions, it has been shown that there is a bias of +5% (Kaufman 2005). The uncertainty associated with MODIS fine mode fraction is estimated at 20% (Remer et al. 2005). The equivalent set of estimates for $\tau_{du,MODIS}$ from the Aqua platform extends from 2003 to 2017. AOD from MODIS TERRA and AQUA have been shown to agree very well (Ichoku 2005). However, over ocean, collection 5 was shown to introduce a 0.015 offset between Terra and Aqua mean MODIS AOD (Remer et al. 2008), and this carries over as a -0.004 bias for Aqua $\tau_{du,MODIS}$ relative to Terra $\tau_{du,MODIS}$. This paper will focus largely on the $\tau_{du,MODIS}$ from the Terra platform, as it is a longer record. However, we will briefly discuss the decadal trends in the $\tau_{du,MODIS}$ derived from Aqua in a later section.

As our $\tau_{du}$ estimate is built upon AOD, it carries with it the known limitations of the sensors from which it is derived. For MODIS, this includes a high bias over turbid coastal waters and errors in locations where the surface wind speed is significantly different from the value of 6 m/s assumed in the product algorithm (Kahn et al. 2007; Kleidman et al. 2012). MODIS AOD retrievals are limited to cloud-free pixels and errors in cloud screening will impact the AOD estimate. The MODIS aerosol cloud mask uses the standard deviation of reflectance in sets of pixels to remove cloudy pixels, which increase spatial variability. Absolute reflectance at 1380 nm and the ratio of reflectances at 1380 nm and 1240 nm, as well as several infrared tests are used for additional screening of thin cirrus. Over ocean, the brightest and darkest 25% of the remaining pixels are arbitrarily removed and the average reflectance in each channel is calculated from these remaining pixels. Over land, the brightest 50% and darkest 30% of pixels are discarded before the averaging step (Remer et al. 2012). While this usually produces a reasonable result, in the case that unscreened clouds remain before the discarding of the brightest and darkest retrievals, this can produce AOD estimates that are biased high (Kahn et al. 2007). It is known that MODIS AOD is biased very high in the southern hemisphere mid to high latitudes over the Southern Ocean due to extensive broken stratocumulus and cirrus cloud contamination (Toth et al. 2013). We have limited these datasets to extend from 60°N to 50°S in order to avoid this region and high latitude regions with

limited coverage due to restrictions on the solar zenith angle for remote sensing retrievals by MODIS and AVHRR.

AEROsol RObotic NETwork (AERONET) O'Neil algorithm fine mode fraction retrievals (accessed at https://aeronet.gsfc.nasa.gov) are used to estimate $\tau_{du,MODIS}$ and $\tau_{du,AVHRR}$ over the ocean. In the determination of AERONET fine mode fraction, two spectral modes of AOD are defined based on the premise that the coarse mode spectral variation is approximately neutral while the derivative of the fine mode spectral variation is an approximate function of the fine mode angstrom exponent (O'Neill 2003). From this, the ratio of fine mode to total AOD is determined at a reference wavelength of 500nm from a second order polynomial fit of the natural logarithm of AOD and wavelength applied to each AOD spectrum, across 6 bands. All AERONET data used here are from the Level 2 products. MODIS FMF has been shown to slightly overestimate the fine mode fraction in dust or salt dominated regions by 0.1 - 0.2 relative to AERONET FMF as generated from the O'Neil algorithm (Kleidman et al. 2005), which has the potential to introduce a small postive bias in our estimated $\tau_{du}$.

MODIS Deep Blue products (AOD, single scattering albedo (SSA), angstrom exponent (AE) accessed at https://ladsweb.modaps.eosdis.nasa.gov) were used in the estimation of $\tau_{du,MODIS}$ over land (Hsu et al. 2013). These products use the blue channels of MODIS, where surface reflectance is very low. Pixel level retrievals are averaged over 10km x 10km grids and data are then aggregated into granuals. In the present study, Collection 6 Level 3 MODIS Deep Blue products were used, which are provided at 1° x 1° resolution. SSA at 412nm and at 660nm were used in addition to AE, which is inversely proportional to particle size (Angstrom 1929). MODIS C6 Deep Blue AOD was used as the basis for estimation of $\tau_{du,MODIS}$ over land and is reported to have an expected error of +(0.04 + 10%) - (0.02+10%) (Hsu et al. 2014). The collection 6 (C6) deep blue AOD release extended coverage to all non-snow land surfaces, where collection 5 only included bright land surfaces.

The AVHRR AOT at 630nm climate data record (CDR) (accessed at https://www.ncei.noaa.gov/data/) was used in the estimation of $\tau_{du,AVHRR}$ (Zhao and Program 2017). The CDR dataset was created using the NOAA AVHRR PATMOS-x Level-2B data product (Zhao et al. 2008, 2002; Zhao and Program 2017). This dataset combines retrievals from 17 different sensors, and the overpass time and number of observations per day (4-8 obs/day) varied between sensors. Large data gaps occur for years before 1985. AVHRR AOT was re-gridded from its native resolution of 0.1° x 0.1° to a resolution of 1°x1° using inverse distance weighted interpolation. Aerosol retrievals are only available over ocean and require clear-sky conditions, which in this case are defined by cloudy probability less than 1%. Cloudy probability is determined through a naive Bayesian cloud detection technique performed on a 3 x 3 pixel grid surrounding a given pixel (Heidinger et al. 2014). The CDR AVHRR AOT dataset has a systematic error of $0.03 \pm 0.006$ and a random error of $\pm 0.113$ (Zhao and Program 2017).

Daily mean surface wind speed from the second Modern-Era Retrospective Analysis for Research and Applications (MERRA-2) (Gelaro et al. 2017) one hour time-averaged surface flux assimilation product (accessed at https://disc.gsfc.nasa.gov/) was used in the estimation of marine AOD. This was re-gridded from its native resolution of 0.625°longitude x 0.5°latitude to a resolution of 1° x 1° using bilinear interpolation. MERRA-2 surface wind patterns have been shown to be similar to other datasets, but greater in magitude in most regions than MERRA and ERA-Interim and weaker in magitude than NCEP-R2 (Bosilovich et al. 2015). Similar to most reanalysis products, MERRA-2 winds are weaker than 93% of observations considered in Bosilovich et al. (2015).

### b. $\tau_{du,MODIS}$ over ocean

$\tau_{du,MODIS}$ over the ocean for the time period between 2001 and 2017 was estimated based on the method of Kaufman (2005), but with several minor modifications. Briefly, assuming that the major contributions to total AOD are anthropogenic aerosol, marine aerosol, and dust aerosol, one can deduce $\tau_{du}$ by estimating the contributions from the other two aerosol types. As anthropogenic aerosols are generally dominated by submicron particles, the ratio of fine mode aerosol optical depth to coarse mode aerosol optical depth, called the fine mode fraction ($f$), can be used to discriminate these types. The total aerosol optical depth ($\tau$) is defined by

$$\tau = \tau_{du} + \tau_{ma} + \tau_{an} \tag{1}$$

where $\tau_{du}$, $\tau_{ma}$, and $\tau_{an}$ are the dust, marine and anthropogenic contributions to the aerosol optical depth, respectively. The fine mode aerosol optical depth is given by $f\tau$, and can be expressed as a function of the fine mode optical depth contributions from the individual aerosol species,

$$f\tau = f_{du}\tau_{du} + f_{ma}\tau_{ma} + f_{an}\tau_{an} \tag{2}$$

where $f$, $f_{du}$, $f_{ma}$, and $f_{an}$ are the total, dust, marine, and anthropogenic contributions to the fine mode fraction, respectively. Equations 1 and 2 can be combined and rearranged to yield the dust aerosol optical depth ($\tau_{du}$):

$$\tau_{du} = \frac{\tau(f_{an} - f) - \tau_{ma}(f_{an} - f_{ma})}{f_{an} - f_{du}} \tag{3}$$

Data sources for each of these variables can be found in Table 1. Characteristic fine mode fraction for marine ($f_{ma}$) , anthropogenic ($f_{an}$), and dust ($f_{du}$) aerosol were determined using the average fine mode fraction from

TABLE 1. Summary of variables and data types used in equations 1, 2, and 3.

| *Variable* | *Platform* | *Instrument* | *Retrieval Wavelength* |
|---|---|---|---|
| $\tau$ | TERRA/NOAA | MODIS/AVHRR | 550 nm or 630 nm |
| $f$ | TERRA | MODIS | N/A |
| $f_{du}$ | AERONET | Sun Photometer (O'Neill method) | 500 nm |
| $f_{ma}$ | AERONET | Sun Photometer (O'Neill method) | 500 nm |
| $f_{an}$ | AERONET | Sun Photometer (O'Neill method) | 500 nm |
| $\tau_{mar}$ | MERRA-2 | Parameterized based on surface wind speed | N/A |

TABLE 2. AERONET stations used for calculation of $f_{an}$, $f_{du}$, and $f_{ma}$ with the years of data used from each station in this calculation.

| *Variable* | *Mean* | *AERONET Stations* |
|---|---|---|
| $f_{an}$ | 0.73 | Alta Floresta (1993-2018), GSFC (1993-2018), Campo Grande (1995), Mongu (1995-2010), Mainz (1997-2018), Abracos Hill (1999-2005), Belterra (1999-2005), Cordoba CETT (1999-2010), CEILAP BA (1999-2018), Palaiseau (1999-2018), Skukuza Aeroport (2000), UCLA (2000-2018), Hamburg (2000-2018), Rio Branco (2000-2018), Philadelphia (2001), CCNY (2001-2018), Cuiaba Miranda (2001-2018), Rome Tor Vergata (2001-2018), Fresno (2002-2012), Billerica (2002-2018), Halifax (2002-2018), New Delhi (2004-2010), Petrolina Sonda(2004-2017), Hong Kong PolyU (2005-2018), HongKong Hok Tsui (2007-2010), Dayton (2008-2018), Hong Kong Sheung (2012-2018). |
| $f_{du}$ | 0.40 | Solar Village (1999-2015), Hamim (2000-2007), Tamanrasset INM(2006-2018), Tamanrasset TMP(2006), Eilat (2007-2018) |
| $f_{ma}$ | 0.36 | Midway Island (2001-2015), Nauru (1999-2013), Amsterdam Island (2002-2018), Crozet Island (2003-2013), ARM Graciosa (2013-2018), American Samoa (2014-2017) |

AERONET stations dominated by each aerosol type (Table 2). MODIS retrievals were not used for determining these coefficients, since fine mode fraction is only distinguishable over the ocean with this instrument making it likely that all MODIS fine mode fraction estimates contain some significant contribution from sea spray. This represents a deviation from the methods of Kaufman (2005).

### 1) MARINE AEROSOL CONTRIBUTION

Kaufman (2005) parameterized marine aerosol based on NCEP surface (1000hPa) wind speed at 2.5° x 2.5° resolution. This parameterization was based on the relationship between surface wind speed from a National Climatic Data Center (NCDC) meteorological station and an AERONET station on Midway Island from 14 months of data, excluding the dust season (February through May) (Smirnov et al. 2003).

Here we have chosen to use MERRA-2 in order to take advantage of a higher resolution reanalysis product, and have updated the equation of the parameterization based on more recent findings regarding the wind speed dependence of marine aerosol. We expect that the wind speed dependence of total marine aerosol is primarily the result of the coarse mode aerosol (Lehahn et al. 2010; Satheesh et al. 2006). The parameterization used here is derived from the relationship between MODIS TERRA coarse mode AOD and MERRA-2 surface wind speed interpolated to a 1°x1° grid in the southern equatorial Pacific (0-25°S, 178-130°W), where it is assumed there is no influence from pollution or dust aerosol, and the mean fine mode AOD in this region (not shown). Based on these data, the fine mode contribution to the total marine aerosol optical depth was independent of wind speed, with a mean of $0.05 \pm 0.03$.

From these reanalysis wind speeds and AOD retrievals over this region in the Equatorial South Pacific, the contribution of marine aerosol ($\tau_{ma}$) to the total aerosol was parameterized based on daily mean MERRA-2 surface wind speed ($w$) according to

$$\tau_{ma} = \tau_{ma,c} + \tau_{ma,f} \tag{4}$$

$$\tau_{ma,c} = 0.007w + 0.02 \tag{5}$$

$$\tau_{ma,f} = 0.05(\pm 0.03) \tag{6}$$

Where $\tau_{ma,c}$ and $\tau_{ma,f}$ are the coarse and fine mode contributions to marine aerosol, respectively. These results are consistent with the findings of Lehahn et al. (2010), which found coarse marine aerosol to be linearly related to surface wind speed with a slope of $0.009 \pm 0.002 m/s$. We investigated the wind speed dependence of marine aerosol using daily mean MERRA-2 surface wind speed and MODIS TERRA coarse and fine mode aerosol at several island stations, including American Samoa, Nauru, and Midway Island, and the results were consistent with the parameterization used here, and were within the range reported in Lehahn et al. (2010) (not shown).

### c. $\tau_{du,MODIS}$ over land

Dust AOD over land for the time period between 2001 and 2017 was estimated based on the methods of Ginoux et al. (2012) with minor modifications. Ginoux et al. (2012) used MODIS deep blue AOD to identify pixels over land that contained dust by their column optical characteristics including deep blue AOD greater than 0.1, angstrom exponent (AE) less than 0, single scattering albedo (SSA) at 412 nm less than 0.95, and SSA at 412nm greater than SSA at 660nm. If a retrieval met each of these criteria, its deep blue AOD contributed to the long-term mean of dust aerosol optical depth at that grid cell. In order to test the thresholds used in Ginoux et al. (2012), we collected these same data within three over-land regions where the aerosol signal is dominated by dust, and one over-land region where mineral aerosols are unlikely to be present, and binned the pixels of this data for each location by their optical properties. The dust-dominated locations included a region over the Sahara desert (10-30°E, 19-30°N) (Figure 1a), a region over the Arabian desert (40-50°E, 23-35°N) (Figure 1b), and a region over the Taklamakan desert (77-88°E, 36-40°N) (Figure 1c). The non-dust dominated location chosen was over equatorial Africa (10-32°E, 10°S-5°N) (Figure 1d).

In all three dust-dominated regions, 98%, or more, of pixels meet the criteria for SSA at 412nm less than 0.95 while in the region dominated by other aerosol types, only 24.22% of pixels meet this criteria. Similarly, in each dust-dominated region, greater than 99% of pixels meet the criteria of SSA at 412nm exceeding or equal to SSA at 660nm, while only 35.95% meet this criteria for the non-dust region. The criteria used in Ginoux et al. (2012) of deep blue AOD greater than 0.1 was not used in the creation of $\tau_{du,MODIS}$ here.

Ginoux et al. (2012) used a conservative requirement of AE less than 0 to identify dust. However, the updated algorithm used to create the C6 deep blue AE product now limits the valid range of values to $0 \geq \text{AE} \leq 1.8$ (Sayer et al. 2013; Hsu et al. 2013). Therefore, we chose a new threshold based on the distribution of AE in our three desert regions. When this threshold was replaced with a criteria of AE less than 0.6, 84.71% of pixels in the Sahara desert region, 65.2% of pixels in the Arabian desert region, and 55.31% of pixels in the Taklamakan desert region met the new threshold while only 3.60% met it in the non-dust region. The new threshold of 0.6 we have used here is within the values of AE reported for dust regimes in Dubovik et al. (2002). In summary, daily estimates of $\tau_{du,MODIS}$ over land grid cells are comprised of the deep blue AOD if that pixel that met the following criteria:

- MODIS TERRA Collection 6 (C6) aerosol angstrom exponent (AE) 470nm-670nm, which is inversely proportional to particle size, less than 0.6
- MODIS TERRA C6 single scattering albedo (SSA) at 412 nm, the ratio of aerosol scattering to extinction coefficients at that wavelength, less than 0.95
- MODIS TERRA C6 SSA at 412 nm greater than or equal to SSA at 660 nm

If a pixel did not meet these criteria, its $\tau_{du}$ was set equal to zero. An analysis of the accuracy of this method, through comparison with AERONET, is presented in Section 3c of this manuscript.

### d. $\tau_{du,AVHRR}$ (1981 - 2017)

$\tau_{du,AVHRR}$ over the ocean from 1981 to 2017 was derived similarly to what was previously described for MODIS. However, AOT from AVHRR was used rather than MODIS AOD, and the climatological seasonal mean fine mode fraction from the MODIS period was used in equation 1. Evan and Mukhopadhyay (2010) showed that over the tropical North Atlantic, a dusty region, the seasonal cycle in the fine mode fraction is far larger than the inter-annual variability, such that monthly climatological mean fine mode fraction can be used in place of monthly-mean fine mode fraction without introducing significant biases. Here we also assume that the use of monthly climatological fine mode fraction can be used in place of daily fine mode fraction. We tested this assumption by calculating the $\tau_{du,MODIS}$ using climatological fine mode fraction and the results were similar to the estimated $\tau_{du,MODIS}$ calculated using daily fine mode fraction, with a bias of 0.00 in the long-term global mean over the ocean for the period 2001-2017 (RMSE: 0.03). The characteristic find mode fractions, $f_{ma}$, $f_{du}$, and $f_{an}$, were the same as those used in the calculation of $\tau_{du,MODIS}$ . Following Evan and Mukhopadhyay (2010), stratospheric aerosol as estimated in Sato et al. (1993) was removed from AVHRR AOT before calculation of $\tau_{du,AVHRR}$ for years prior to 1999 and was assumed to be zero in subsequent years.

The global mean time series of $\tau_{du,AVHRR}$ created by this method contained very large fluctuations in years prior to 1995 related to the impact of satellite drift on AVHRR AOT (Figure 2). This problem has previously been noted

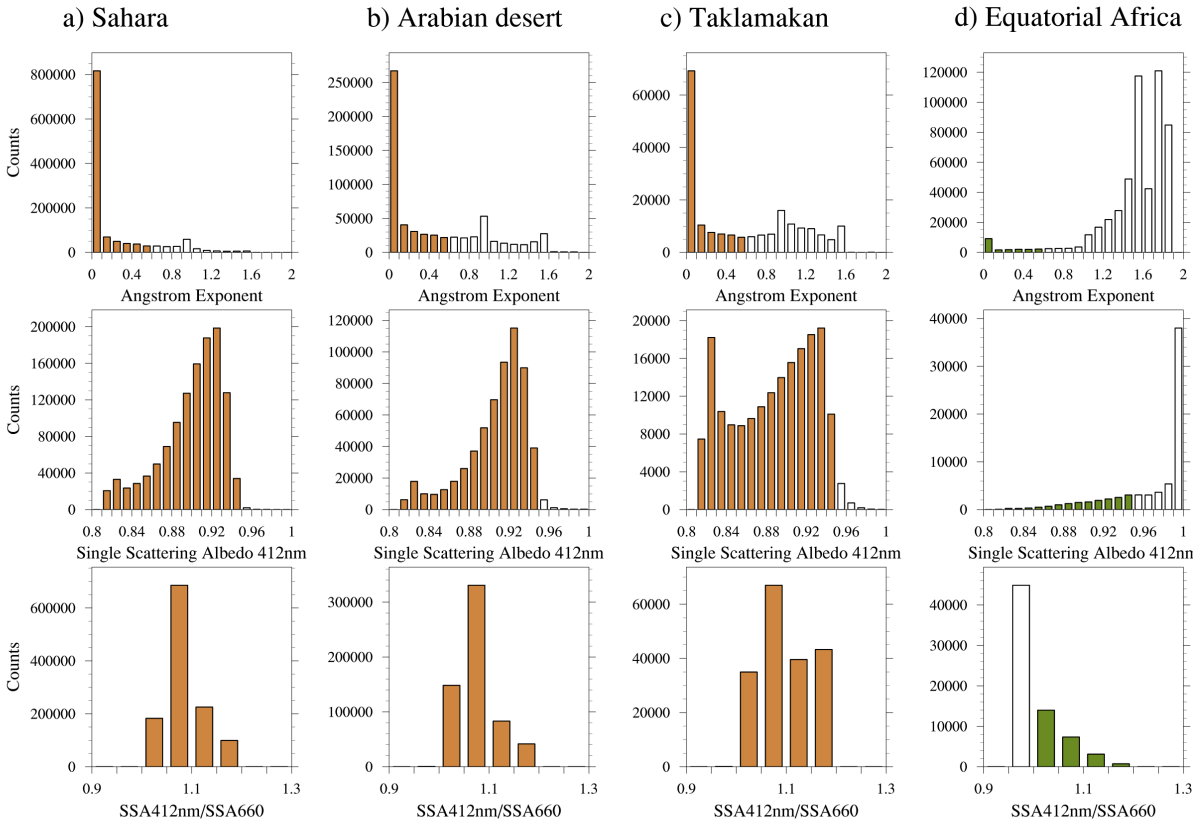


FIG. 1. Histograms of Angstrom Exponent (top), Single Scattering Albedo (middle), and ratio of Single Scattering Albedo at 412 nm divided by Single Scattering Albedo at 660nm (bottom) for three characteristically dusty regions a) the Sahara desert (10-30°E,19-30°N), b) the Arabian desert (40-50°E,23-35°N), and c) the Taklamakan desert (77-88°E,36-40°N), and one anthropogenic aerosol dominated region, d) Equatorial Africa (10-32°E,10°S-5°N) for the period from 2001 to 2017. Colored green (1a-c) or brown (1d) bars indicate bins that match the criteria used to identify dust for the respective optical property.

in the long-term AVHRR records of cloud cover (Foster and Heidinger 2013; Norris and Evan 2015). In order to remove this signal, following the method of Norris and Evan (2015), we regressed the monthly global mean time series of $\tau_{du,AVHRR}$, with the seasonal cycle removed, onto the time series of monthly-mean $\tau_{du,AVHRR}$ at each grid point, with the seasonal cycle removed, and then subtracted the product of the regression coefficient and the global mean time series, with seasonal cycle removed, from the de-seasoned $\tau_{du,AVHRR}$ at each grid point before adding the seasonal cycle back in. While this results in a global DAOD trend of zero, a limitation of this method, it removes variability caused by satellite drift in equatorial crossing time, changes in satellite zenith angle, and unrealistically large anomalies associated with instrument calibration problems and does not have a significant impact on regional variability or regional trends.

### e. *Uncertainty Analysis*

In order to evaluate how constrained our DAOD estimates are, we calculated the uncertainty on each estimate of $\tau_{du,MODIS}$ and $\tau_{du,AVHRR}$ over water. These datasets may be applied in the future for evaluation of dust in

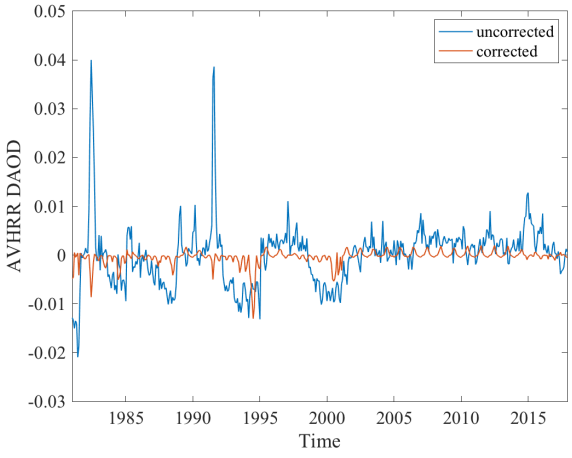


FIG. 2. Uncorrected global mean time series of $\tau_{du,AVHRR}$ with seasonal cycle removed (blue) and global mean time series of $\tau_{du,AVHRR}$ after correction for orbital drift (red).

climate models, and an estimate of uncertainty on our observations-based $\tau_{du}$ may be useful in understanding whether modeled dust is within the distribution of observed $\tau_{du}$. The climatological mean uncertainty associated with each grid box over water in the $\tau_{du,MODIS}$ was estimated by propagating the $1\sigma$ error associated with each term in equations 3 and 4. The standard deviation of all AERONET fine mode fraction measurements used in the calculation of $f_{ma}$, $f_{an}$, and $f_{du}$ was taken as the uncertainty in those coefficients. The expected error in MODIS AOD and in MODIS fine mode fraction were used as the uncertainty associated with those terms. The marine aerosol uncertainty term is calculated from the standard error of the regression coefficient for the linear relationship between coarse AOD and wind speed in the southern equatorial Pacific (0-25°S, 178-130°W) from 2001 to 2017 and the standard deviation of the fine mode AOD there. The uncertainty associated with this $\tau_{du}$ estimate scales with magnitude of AOD and, as a result, is highest in dusty regions such as the equatorial Atlantic and near to the Arabic Peninsula (not shown). Fractional error is lowest in these regions, and very high fractional error occurs in regions where dust does not frequently occur (ie. where climatological $\tau_{du}$ is very low). The long-term mean global $\tau_{du,MODIS}$ over the ocean was found to be $0.03 \pm 0.06$, which accounts for the variance in the global mean time series of $\tau_{du,MODIS}$ and the $1\sigma$ errors for each pixel. We note that $\tau_{du}$ does not follow a gaussian distribution. This global mean and $1\sigma$ error were calculated using a closed-form equation. However, we obtain the same result when calculating this mean and uncertainty using Monte-Carlo methods.

The uncertainty associated with the $\tau_{du,AVHRR}$ was calculated in the same manner as the $\tau_{du,MODIS}$ over-water. However, the random error in AVHRR AOT was used, rather than the expected error in $\tau_{du,MODIS}$, and the uncertainty associated with the use of climatological fine mode fraction was estimated by adding in quadrature the expected error in MODIS fine mode fraction, and the standard deviation of fine mode fraction estimates used in calculating the climatological fine mode fraction. The long-term mean global $\tau_{du,AVHRR}$ over ocean was found to be $0.02 \pm 0.10$.

The uncertainty associated with $\tau_{du,MODIS}$ over land could be assumed to be the expected error in the MODIS Deep Blue aerosol optical depth at 550 nm, since the $\tau_{du}$ at any grid cell that matched the optical properties indicative of dust is equal to the the Deep Blue AOD at that grid cell. However, in order to evaluate the accuracy of our identification, we created three time-series datasets of dust from AERONET stations in regions with different characteristic aerosol types. The first, the Tamanrasset station (2006), we consider to be a dusty region as it is in the Sahara desert. The second, the Mainz station (2003-2017), we consider to be an anthropogenic aerosol-dominated region in Germany. The third, the Ilorin station (2001-2017), we consider to be a mixed polluted dust region in the southern Sahel. For each of these stations, AERONET daily mean Angstrom Exponent (AE 440nm-870nm) less than 0.5 was used to identify dust, and AE 440nm-870nm greater than 1 was used to identify days without dust. This choice was consistent with Giles et al. (2012), which found that AERONET extinction AE 440nm-870nm for most of the dust-dominated stations analyzed had values of $0.3 \pm 0.2$ while , anthropogenic aerosol-dominated stations had values equal to or exceeding 1. We chose a different threshold than what was used to estimate $\tau_{du,MODIS}$ over land because AERNONET AE is measured at different wavelengths than AE from MODIS, and we wanted to remain consistent with what is published specifically for the AE using these wavelengths. This binary classification (dust or no dust) for each station was compared with time series of $\tau_{du,MODIS}$ at the closest grid cell to each station, with any $\tau_{du,MODIS}$ greater than zero considered as a dust classification and any $\tau_{du,MODIS}$ equal to zero, a no dust classification. The results of this analysis are presented in Table 3. False positives are less than 5% in all cases, with 0% occurence of false postives for the polluted region. Missed dust occurences are high (35%) in the pollution and dust mixed region and about 10% occurence in the dusty region. This is consistent with our hypothesis that this method would have the least skill in regions where dust is heavily mixed with pollution. Including a requirement of Deep Blue AOD greater than or equal to 0.1, as is done in Ginoux et al. (2012) would increase misses to 18% occurrence in the dusty region.

TABLE 3. Quantified skill for $\tau_{du,MODIS}$ over land in regions with differente dominant aerosol type. AERONET daily mean Angstrom Exponent (440nm-870nm) less than 0.5 was used as ground truth to identify dust and greater than 1 was used to identify non-dust aerosol.

| *Region type* | *Station* | *Accuracy (dust)* | *Accuracy (no dust)* | *Missed* | *False Positive* |
|---|---|---|---|---|---|
| *Dusty* | Tamanrasset (22.79°N, 5.530°E) | 86.29% | 9.43% | 10.32% | 3.81% |
| *Polluted* | Mainz (49.99°N, 8.4°E) | 12.5% | 95.21% | 0.70% | 4.41% |
| *Mixed* | Ilorin (4.675°N, 8.484°E) | 15.63% | 100% | 35.11% | 0% |

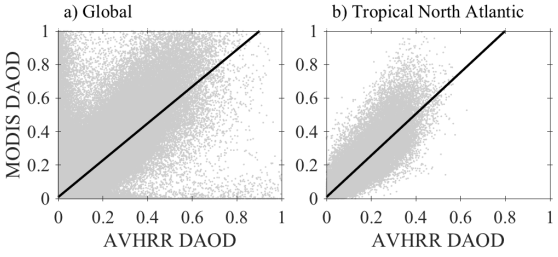


FIG. 3. Scatter of monthly mean $\tau_{du,MODIS}$ and $\tau_{du,AVHRR}$ *a*) globally, and *b*) for a region over the tropical Atlantic (5°S-20°N, 20-30°W) for the period from 2001 to 2017. The solid black line is the best fit to a linear form. *a*) Globally, this is the fit to $y = 1.10(\pm 0.002)x + 0.009$ with a corrected r-squared value of 0.48, RMSE equal to 0.07, and SSE of 15010. *b*) In the tropical Atlantic, this fits the equation $y = 1.24(\pm 0.006)x + 0.009$ with a corrected r-squared value of 0.74, root mean squared error (RMSE) equal to 0.08 and summed square of residuals (SSE) equal to 362.30.

## 3. Results

The primary results of this work are two near-global, daily, observational datasets of $\tau_{du}$ at 1° x 1° resolution that can be used for studies of dust transport, trends, and physical processes, including one dataset that covers both water and land surfaces. The remainder of this section will be used to discuss *a*) a comparison of $\tau_{du,AVHRR}$ and $\tau_{du,MODIS}$, *b*) a description of seasonal climatological mean $\tau_{du}$, *c*) verification of $\tau_{du,MODIS}$ against ground-based measurements of dust aerosol, and *d*) trends in $\tau_{du}$ as an example of the utility of this dataset.

### *a. Comparison of MODIS and $\tau_{du,AVHRR}$*

Globaly, monthly mean estimates of $\tau_{du,MODIS}$ and $\tau_{du,AVHRR}$ are related by the linear least squares best-fit to y = 1.10x + 0.009 ($r^2$ = 0.48, RMSE:0.07, Bias: -0.01) (Figure 3a). However, it is useful to compare these two estimates in a region that is characteristically dust-dominated. In the tropical North Atlantic, a dusty region, they linearly related with a form y = 1.24x + 0.009 ($r^2$ = 0.74, RMSE:0.08, Bias: -0.04) (Figure 3b). Monthly mean $\tau_{du,AVHRR}$ is biased low (Bias:-1.18) compared to $\tau_{du,MODIS}$ for $\tau_{du,MODIS}$ greater than unity. We hypothesize that the low bias in $\tau_{du,AVHRR}$ is an artifact of misclassification of optically thick dust layers as clouds in the AVHRR AOT cloud clearing algorithm (Xuepeng Zhao, personal communication, April 18, 2018), although it also could have been a result of the difference wavelengths between MODIS AOD retrievals and AVHRR AOT retrievals (Zhao et al. 2008). In order to test this, we also calculated the linear least squares best-fit between the daily $\tau_{du,MODIS}$ and daily $\tau_{du,AVHRR}$. We expect that if the low bias of $\tau_{du,AVHRR}$ relative to $\tau_{du,MODIS}$ is due to missing data in regions of optically thick dust, rather than due to the difference in wavelength, the slope of the regression between these datasets will be significantly less steep for the daily data than for the monthly data in the tropical North Atlantic. Indeed, we found that the daily $\tau_{du,MODIS}$ and daily $\tau_{du,AVHRR}$ are related by the relationship y = 0.93x + 0.05 ($r^2$ = 0.46, RMSE:0.15, SSE: 7439, Bias: -0.03) in the tropical North Atlantic, which is a significant 0.31 difference in slope (not shown).

The discrepancy in retrievals over large dust plumes can be easily visualized in the case of June 27th, 2014, over the tropical Atlantic (Figure 4). In this case, $\tau_{du,MODIS}$ indicates an optically thick dust plume, centered near 15°N, 30°W, that has been advected over the tropical Atlantic from the Sahara (Figure 4a). This particularly strong event allowed for dust to be measured in-situ as far as Colombia (Bedoya et al. 2016). In figure 4, grid cells that are missing estimates of $\tau_{du}$ or AOD, or grid cells over land, are masked in grey. For the same day, the $\tau_{du,AVHRR}$ (Figure 4b) is largely missing estimates in the region of optically thick dust. This is a result of missing retrievals of AVHRR AOT (Figure 4d), which occur due to a combination of sun glint and because of the cloud-screening algorithm which may be classifying optically thick dust as cloud.

Geographically, MODIS and $\tau_{du,AVHRR}$ are well correlated (r $>$ 0.70) in high $\tau_{du}$ regions including the equa-

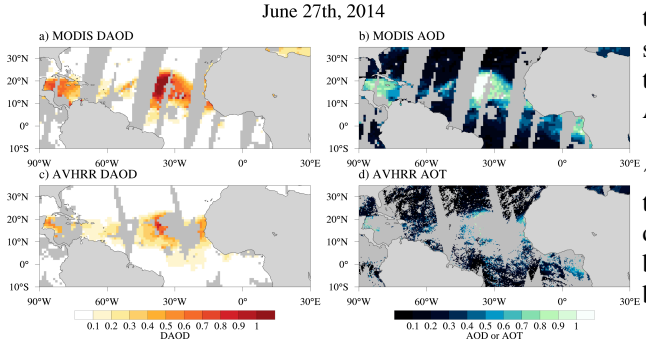


FIG. 4. June 27th, 2014 MODIS *a*) $\tau_{du}$ and *b*) AOD from the Terra platform and AVHRR *c*) $\tau_{du}$ and *d*) AOT. Retrievals and estimates over land and locations where there is missing data are shown in grey.

torial Atlantic, and the Indian Ocean near to the Arabian Peninsula (not shown). MODIS and $\tau_{du,AVHRR}$ are not statistically significantly correlated ($r < 0.19$) in characteristically low $\tau_{du}$ regions, where dust may be transient and detectable only at the overpass time of one of the sensors.

For the remaining analysis, a correction in the form $\tau_{du,AVHRR,corrected} = 1.24\tau_{du,AVHRR,raw}$ is applied to the monthly-mean $\tau_{du,AVHRR}$ based on the linear best-fit to $\tau_{du,MODIS}$ in the tropical North Atlantic as described in the first paragraph of this section. We chose to base the correction on a dusty region because we expect most applications of this dataset to be in dusty regions.

### *b. Seasonal Dust AOD*

Maximums in seasonal mean $\tau_{du,MODIS}$ are found over the Sahara and the Arabic Peninsula in austral summer (JJA) (Figure 5a), and the Taklamakan and Gobi deserts during spring (MAM) (Figure 5c). Aeolian transport from the Sahara towards the Americas is visible during all seasons with a maximum extension westward during the summer (Figure 5d,h), which is well known (Prospero and Mayol-Bracero 2013; Prospero et al. 1996). The Spring maximum in dust aerosol over Asia can be attributed to the high frequency of cold air outbreaks that cause the Mongolian cyclonic depression and frontal systems in that season, when synoptic systems are unstable and the climate is at its driest (Sun et al. 2001; Ge et al. 2014). During this season, dust is transported from the Asian continent over the North Pacific Ocean towards North America at latitudes between 30°N and 50°N. It is presumed that this dust is primarily from the Taklimakan desert as the local topographical and meteorological conditions allow for it to be entrained to elevations exceeding 5km while dust from the Gobi desert is, for the most part, confined closer to the surface (<3km) (Sun et al. 2001). It has also been shown that some portion of this trans-Pacific dust originates from Africa (Creamean et al. 2013).

Seasonal mean $\tau_{du,AVHRR}$, appears far lower than $\tau_{du,MODIS}$ near to major dust sources in all seasons, due to limited retrievals in regions of optically thick dust as described in the previous section. However, the correction based on comparison with $\tau_{du,MODIS}$ greatly reduces this bias (Figure 5e-h).

Discrepancies between $\tau_{du,MODIS}$ over land and $\tau_{du,MODIS}$ over adjacent ocean are visible in some areas with significant anthropogenic aerosol sources, including the Sahel region of Africa and India during austral fall and spring (Figure 5b,c). This may be due to different methods and data sources used for estimating $\tau_{du,MODIS}$ over land and ocean. The method used for $\tau_{du,MODIS}$ over the ocean leads to a continuous range of $\tau_{du,MODIS}$, whereas the threshold approach used for estimation of $\tau_{du,MODIS}$ over land may prevent these gradients when there is significant mixing between anthropogenic aerosols and dust aerosol. However, this may also partially be the result of the different algorithms used in the retrieval of AOD over land and ocean (Sayer et al. 2013; Hsu et al. 2013). While these unphysical discrepancies could be avoided through spatial interpolation across these boundaries, we have chosen not to do this in order to minimize our assumptions and retain a daily dataset that is directly representative of the satellite observations.

Summertime trans-Pacific transport of dust has been occasionally observed previously (Yumimoto et al. 2010). However, visual inspection of MODIS TERRA corrected reflectance on days when $\tau_{du,MODIS}$ over the western North Pacific (Figure 5c) was high during summer months yielded indications of contamination from biomass burning over Europe and Russia. We compared summer seasonal mean $\tau_{du,MODIS}$ and MERRA-2 organic carbon extinction optical thickness at 550nm (not shown, accessed at https://giovanni.gsfc.nasa.gov/) and confirmed that summer seasonal mean organic carbon was highest over the western North Pacific in years when summer seasonal mean $\tau_{du,MODIS}$ was highest, supporting the hypothesis that there may be biomass burning contamination over the western North Pacific during these months. The fine mode fraction ($f$) during these summer high $\tau_{du,MODIS}$ events is approximately $0.57 - 0.63$ which is greater than the characteristic fine mode fraction for dusty regions ($f_{du} = 0.40$). However, it is less than the characteristic fine mode fraction for anthropogenic aerosol-dominated regions ($f_{an} = 0.73$), allowing some small portion of the

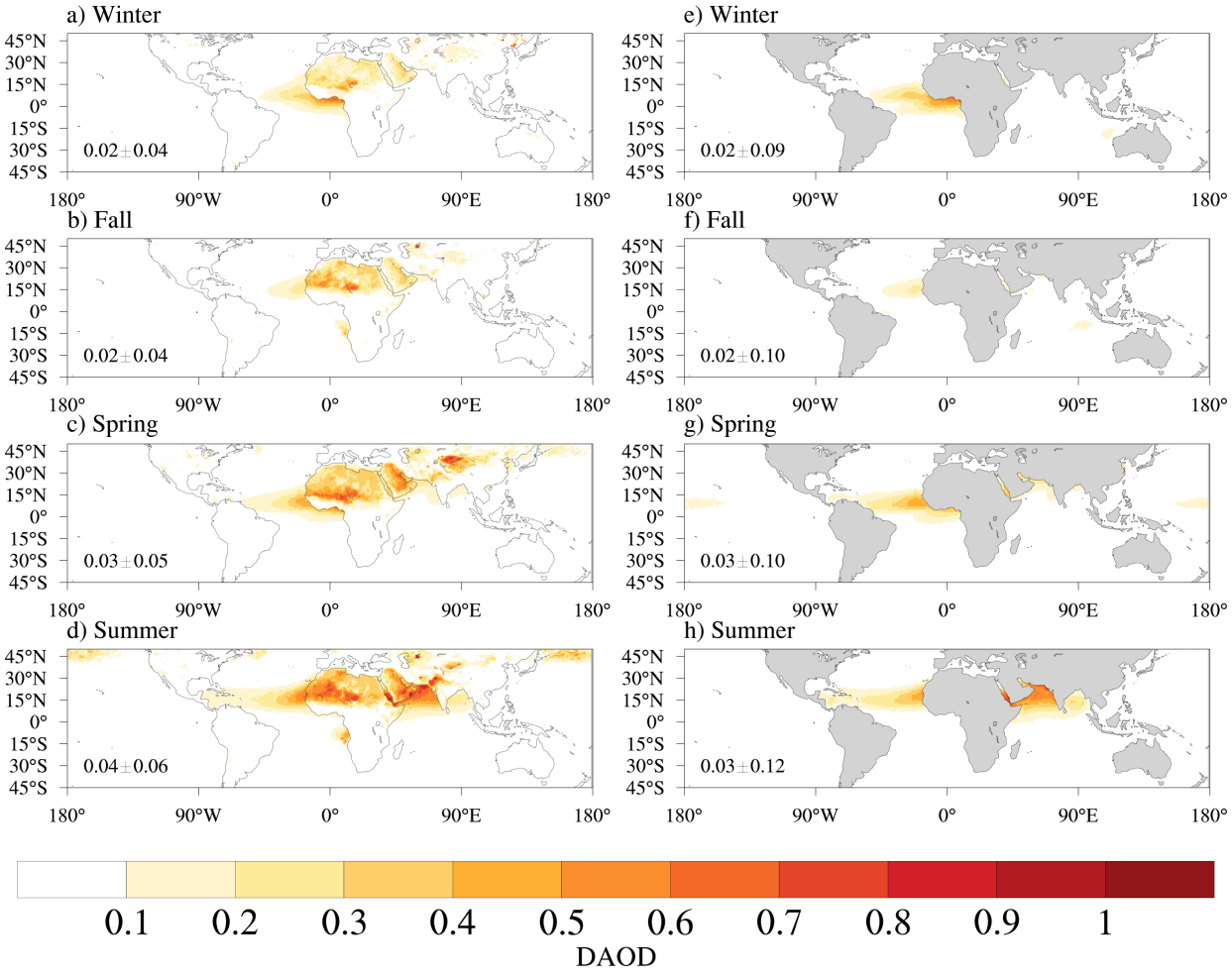


FIG. 5. Seasonal mean $a-d$) $\tau_{du,MODIS}$ averaged over the period from 2001 to 2017 and $e-h$) $\tau_{du,AVHRR}$ over the period from 1981 to 2017. The long-term global mean $\tau_{du} \pm 1\sigma$ uncertainty over the ocean for each season and dataset is featured in the bottom left-hand corner of each panel.

MODIS AOD for that pixel to contribute to $\tau_{du,MODIS}$ if it exceeds the contribution from marine aerosol. When the MODIS AOD is very large, this can lead to a significant contribution to $\tau_{du,MODIS}$. In the springtime, most of the high $\tau_{du,MODIS}$ events are associated with fine mode fractions near 0.50, which is closer to $f_{du}$

In addition, this region in the western North Pacific has few retrievals during the summer months, as extensive low clouds cover that area. The limited number of retrievals is evident in the number of pixels used in the estimate of MODIS Dark Target AOD during the summer in that region (not shown). While greater than 36 pixels are incorporated on average in the equatorial Pacific estimations of MODIS Dark Target AOD, only approximately 26 on average are used in this estimation in parts of the western North Pacific. This signal was not present in the $\tau_{du,AVHRR}$ (Figure 5c-f).

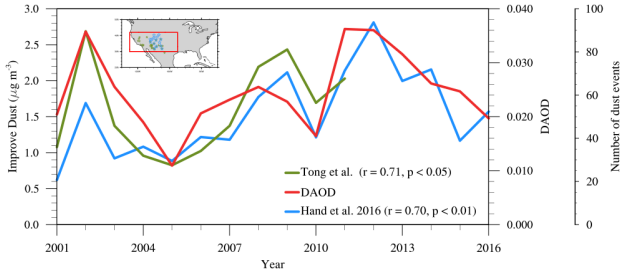


FIG. 6. Annual mean $\tau_{du,MODIS}$ from land grid points in the Southwestern United States within the region shown in the red box (125-95°W, 30-42°N), compared with number of dust events annually in the southwestern U.S. as reported in Tong et al. (2017) (green) and dust concentration from IMPROVE sites in the southwestern U.S. as reported in Hand et al. (2016) (blue). IMPROVE stations used in the Tong et al. (2017) analysis are marked with green stars on the inset map, while stations used in the Hand et al. (2016) analysis are marked with blue stars. There are several overlapping stations.

### c. Comparison with existing datasets

It is informative to compare our $\tau_{du}$ to previously published estimates of atmospheric dust. Here, we compare $\tau_{du,MODIS}$ with two recently published time series of dust concentrations over the western U.S. (Tong et al. 2017; Hand et al. 2016) and one over the Caribbean (Prospero and Nees 1986; Prospero et al. 1996). The measurements of dust over the western U.S. are based on surface concentrations of aerosol species. In Hand et al. (2016), Fe from IMPROVE stations was used a proxy for fine dust concentrations and $\tau_{du,MODIS}$ compares well with these annual mean fine dust concentrations ($r = 0.71$, $p < 0.01$) (Figure 6). In Tong et al. (2017), high $PM_{10}$ and $PM_{2.5}$ concentrations, a low ratio of $PM_{2.5}$ and $PM_{10}$, high concentrations of crustal elements (SI, CA, K, Fe, and Ti), low concentration of anthropogenic components, and low enrichment factors of anthropogenic pollution elements from IMPROVE data were used to confirm dust events that had previously been detected in satellite imagery. Annual mean $\tau_{du,MODIS}$ also correlates well with these estimates of annual number of dust events ($r = 0.71$, $p < 0.05$). Although $\tau_{du}$ is a measure of column integrated aerosol, we still expect surface concentrations to be correlated with column integrated values, especially when averaged over a large region. Interestingly, while an increasing trend in dust was noted for these studies for the period between 2001 and 2015, extension of the timeseries through 2017 indicates that dust has been decreasing since 2011.

In order to evaluate the performance of the $\tau_{du,MODIS}$ dataset over the Caribbean, we compared it with independent, ground-based dust measurements at Ragged Point (Prospero and Nees 1986; Prospero et al. 1996). These measurements are based on ash residue from extracted filters with an adjustment factor based on average crustal abundance of Aluminum in soil dust. These data have a standard error that is approximately constant at $\pm 0.1 \mu g m^{-3}$ for concentrations less than 1 $\mu g m^{-3}$ and about $\pm 10\%$ for higher concentrations. We found that in addition to matching the seasonal cycle of dust at this location with a peak in June (Figure 7b), monthly-mean $\tau_{du,MODIS}$ over Barbados is well correlated ($r = 0.53$, $p < 0.01$) with monthly-mean ground-based dust aerosol measurements when the seasonal cycle is removed from both time series (Figure 7a).

## 4. Discussion

### a. Trends in $\tau_{du,MODIS}$

Figure 8 presents decadal trends in monthly mean $\tau_{du,MODIS}$ globally between 2001 and 2017, with the seasonal cycle removed. A trend of increasing $\tau_{du,MODIS}$ of 0.1 units per decade exists over parts of the Arabic peninsula for the MODIS period, consistent with what has been documented in the previous literature (Hsu et al. 2012). Parts of the Saharan desert appear to be getting dustier. However, coastal Northern Africa and the edges of the Sahara display decreasing trends in $\tau_{du,MODIS}$ (Figure 8). Hsu et al. (2012) presented indications that total AOD over northern China was decreasing over the period from 1998 to 2010. However, the decrease was not statistically significant. Our results show a statistically significant decrease in dust aerosol over Northern China and over Southwest Asia indicating that the insignificance of the previously discovered trend may have been due to competing effects of increasing anthropogenic aerosol while dust aerosol was decreasing. Our results are in agreement with recent findings by Pandey et al. (2017) that pre-monsoon dust loading decreased between 2000 and 2015, though this study only analyzed the pre-monsoon months from March through May. The decrease has been linked to increased rainfall, leading to wet scavenging and increased soil moisture, and, to a lesser extent, decreased wind strength over the region for that period. The decrease in $\tau_{du,MODIS}$ over northeast Asia may also be the continuation of a documented decreasing trend from the late 1950s through the 1980s in the region due to reduced cyclone frequency (Qian et al. 2002).

Interestingly, the greatest increase in $\tau_{du,MODIS}$ (1.04 units/decade) is seen over the Aral Sea at the intersection of Kazakhstan and Uzbekistan (44.5°N, 59.5°E). This was once the location of one of the worlds largest lakes, spanning over 66,000 $km^2$ (Izhitskiy et al. 2016). However, the lake has been drying up since the early 1960s, when irrigation projects diverted the rivers that fed it leaving behind a highly emissive exposed playa. The eastern basin of the lake dried up completely in 2014, but the northern parts

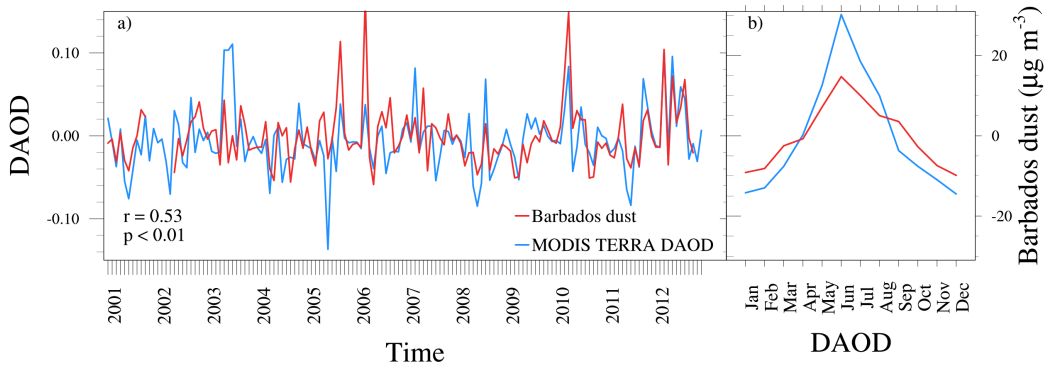


FIG. 7. *a*) Time series of monthly mean ground based dust aerosol measurements on Barbados (red) compared with $\tau_{du,MODIS}$ over Barbados (blue), each with the seasonal cycle removed. *b*) Climatological monthly mean, with long-term mean removed, of measurements on Barbados (red) and of $\tau_{du,MODIS}$ over Barbados (blue)

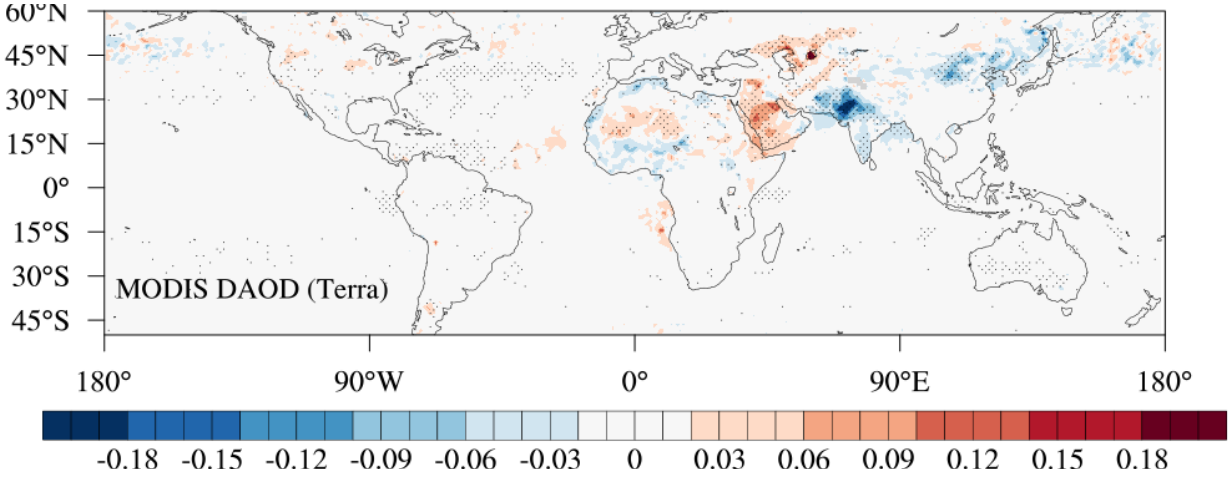


FIG. 8. Trend in $\tau_{du,MODIS}$ over the period 2001-2017 with the seasonal cycle removed. Stippled areas indicate significance at the 95% confidence level.

of the sea remain filled and have largely stabilized. A dramatic increase in $\tau_{du,MODIS}$ is also seen over Razzaza Lake in Iraq, where the shoreline is receding due to diverted irrigation water. The northern-most region of the Caspian Sea, which is also the shallowest portion of the sea, shows a smaller but significant increase in $\tau_{du,MODIS}$ potentially due to the recession of this body of water over the past two decades (Chen et al. 2017).

$\tau_{du}$ derived from MODIS Aqua displays the same trends of decreasing dust over northeast China and southwest Asia and increasing trends over the Arabic Peninsula and Central Sahara (Figure 9). However, there are some regional changes that are more clear in this record, including a statistically significant increase in $\tau_{du}$ over Southern California. There is also an increase in dust over Oman that is not present in the $\tau_{du,MODIS}$ derived from Terra and a greater increase over Iran than is present in the $\tau_{du,MODIS}$ derived from Terra. Differences in regional trends between these two datasets are likely to due the differences in overpass time for the two satellites from which the dataset are derived as it relates to the daily cycle of dust emission. Terra has a morning orbit while Aqua has an afternoon orbit (Ichoku 2005).

The decadal trend in $\tau_{du}$ from 1981 to 2017 over water was also calculated using monthly mean $\tau_{du,AVHRR}$ with the seasonal cycle removed (not shown). This yielded an increasing trend in $\tau_{du,AVHRR}$ near to the Arabian Peninsula, consistent with $\tau_{du,MODIS}$ and with the published literature. This analysis also yielded a decreasing trend in $\tau_{du,AVHRR}$ in the tropical North Atlantic near to the African coast, consistent with the time series of dust at Cape Verde created using a similar method (Evan and Mukhopadhyay 2010). No other trends appeared in the $\tau_{du,AVHRR}$ dataset from 1981 to 2017.

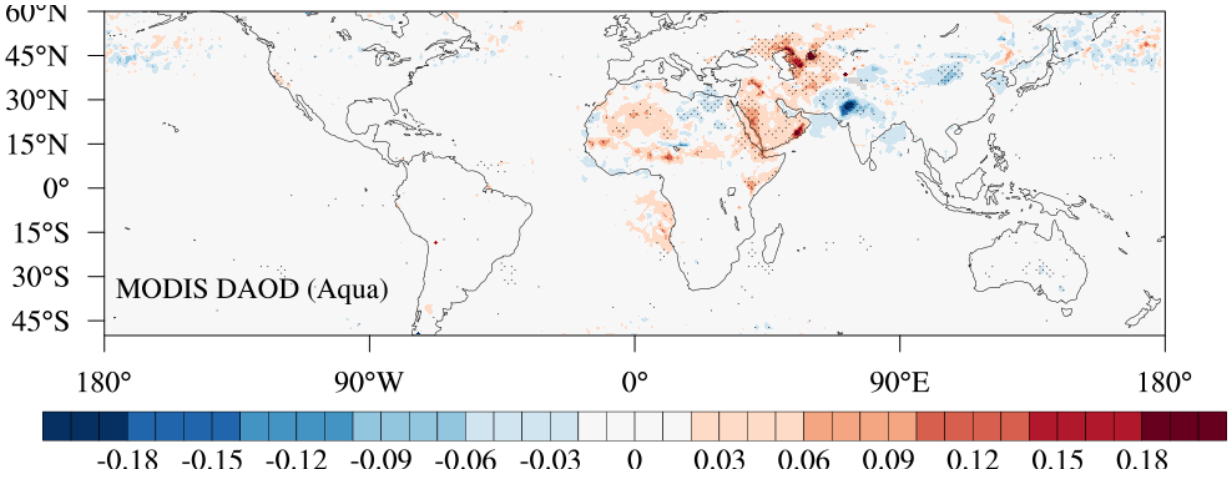


FIG. 9. Same as figure 8 but for $\tau_{du,MODIS}$ derived from Aqua.

*b. Comparison with a modern reanalysis dust product*

In order to understand how this observational dataset compares with a modern reanalysis dust product, we compared $\tau_{du,MODIS}$ to MERRA-2 dust extinction aerosol optical thickness at 550nm (accessed at https://giovanni.gsfc.nasa.gov/giovanni/) over two of the regions, Barbados and the southwestern U.S., used previously in our comparisons with ground observations (Figure 6). Our monthly mean $\tau_{du,MODIS}$, with the seasonal cycle removed, was comparable to the monthly mean MERRA-2 dust extinction aerosol optical thickness over Barbados and to the ground observations from that location (Figure 10a). However, the annual mean $\tau_{du,MODIS}$ displays greater inter-annual variability and was much more similar to the ground observational record than the MERRA-2 dust extinction aerosol optical thickness over the southwestern U.S. (Figure 10b). The similarity of the $\tau_{du,MODIS}$ to the MERRA-2 dust product over barbados likely occurs because the MERRA-2 dust extinction aerosol optical thickness assimilates MODIS Dark Target radiances, which our $\tau_{du,MODIS}$ is based upon, and assimilates data from AERONET stations including one located at Ragged Point, the location where the ground based dust measurements from Prospero et al. (1996) were made. The MERRA-2 product does not assimilate MODIS Deep Blue products over land, instead relying upon a combination of MODIS Dark Target retrievals, Multi-angle Imaging SpectroRadiometer (MISR) AOD retrievals over bright surfaces, and AERONET stations (Randles et al. 2017) which may be sparse in the southwestern U.S. Our $\tau_{du,MODIS}$ dataset appears more representative of observations over land than this reanalysis product, and may be a more appropriate choice for identification and monitoring of dust source regions, particularly those that do not have many AERONET stations.

## 5. Conclusion

These global, daily observationally-based datasets of dust aerosol optical depth will enable a more complete understanding of the complex interactions of dust with weather, climate, and the human system. They are rooted in observations of optical characteristics of the aerosol column from Terra MODIS and from AVHRR, but incorporate observations of characteristic fine mode fraction in dusty, clean marine, and anthropogenically dominated regions from AERONET as well as surface wind speed from MERRA-2 reanalysis. $\tau_{du,MODIS}$ and $\tau_{du,AVHRR}$ are provided at 1° x 1° resolution within the latitude range from 50°S to 60°N. The long-term mean global $\tau_{du,MODIS}$ over the ocean was found to be $0.03 \pm 0.06$. While there are few measurements of dust aerosol for comparison, it compares well with ground-based measurements of dust from the IMPROVE network in the western United States.

While we hoped to create a reliable dataset of $\tau_{du,AVHRR}$ extending from 1981 to 2017 using AVHRR AOT from the CDR AOT dataset, we found that the AVHRR AOT had limited coverage in dusty regions. This limited coverage results in a low bias in seasonal and monthly mean $\tau_{du,AVHRR}$ when compared with $\tau_{du,MODIS}$. However, this was mitigated through the use of a correction factor. We found that $\tau_{du,MODIS}$ increased in the central Sahara and the Middle East, and decreased over northern China and southwestern Asia between 2001 and 2017. The largest increase in dust aerosol optical depth occurred over the Aral Sea which has receded, leaving emissive playa surfaces exposed. We found decreasing decadal trends in $\tau_{du,AVHRR}$ near to Africa in the equatorial Atlantic, and increasing trends near to the Arabian Peninsula from 1981 to 2017. To our knowledge, this work represents the first daily, near-global observational dataset of $\tau_{du}$. As such, it

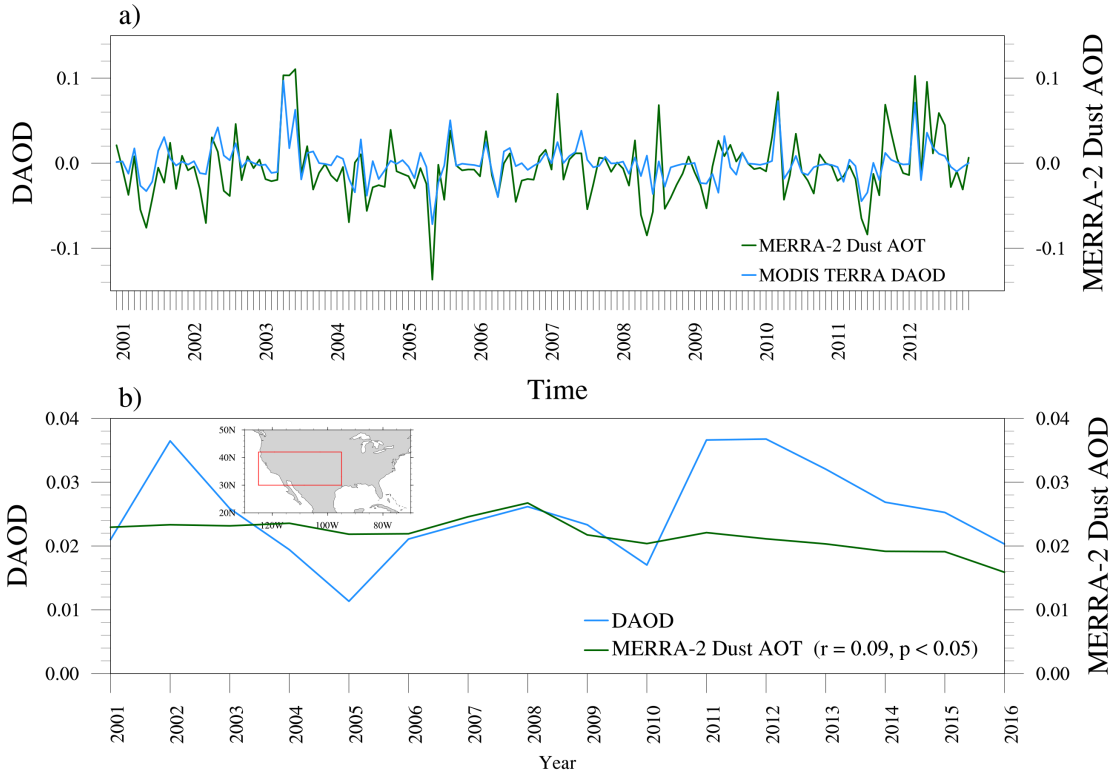


FIG. 10. *a*) Monthly MERRA-2 dust extinction aerosol optical thickness at 550nm and monthly mean $\tau_{du,MODIS}$ over Ragged Point, Barbados between 2001 and 2013 with the seasonal cycle removed. *b*) Annual mean MERRA-2 dust extinction aerosol optical thickness at 500nm and annual mean $\tau_{du,MODIS}$ over the southwestern U.S. from 2001 to 2016.

may be useful for validation of modeled dust aerosol optical depth as well as for physical process studies.

*Acknowledgments.* This work was funded by the California Department of Water Resources contract 4600010378, Task Order *OSCOP*215 and the Army Corps of Engineers USACE (CESU) $W912HZ-15-0019$. We thank the AERONET PIs and their staff for establishing and maintaining the 39 sites used in this investigation. We thank Dr. Joseph Prospero, Dr. Jennifer Hand, and Dr. Daniel Tong for their contributions of long term datasets for comparisons made in this work, and Dr. Martin Ralph, Dr. Leah Campbell and Dr. Nora Mascioli for helpful comments on this manuscript. The datasets described in this manuscript will be made publicly available at Pangea Open Access doi: XXXXXXXXX.

## References

Ai, N., and K. R. Polenske, 2008: Socioeconomic impact analysis of yellow-dust storms: An approach and case study for Beijing. *Economic Systems Research*, **20 (2)**, 187–203, doi:10.1080/09535310802075364.

Angstrom, A., 1929: On the atmospheric transmission of sun radiation and on dust in the air. *Geogr. Ann.*, **11**, 1.

Ault, A. P., C. R. Williams, A. B. White, P. J. Neiman, J. M. Creamean, C. J. Gaston, F. M. Ralph, and K. A. Prather, 2011: Detection of Asian dust in California orographic precipitation. *Journal of Geophysical Research*, **116 (D16)**, doi:10.1029/2010jd015351.

Bedoya, A., and Coauthors, 2016: Strong Saharan dust event detected at Lalinet LOA-UNAL station, over Medellín, Colombia by active and passive remote sensing. *EPJ Web of Conferences*, **119**, 08 006, doi:10.1051/epjconf/201611908006.

Bosilovich, M. G., and Coauthors, 2015: MERRA-2: Initial evaluation of the climate, technical report series on global modeling and data assimilation. Tech. rep., National Aeronautics and Space Administration, Goddard Space Flight Center.

Brown, J. K. M., 2002: Aerial dispersal of pathogens on the global and continental scales and its impact on plant disease. *Science*, **297 (5581)**, 537–541, doi:10.1126/science.1072678.

Chen, G., and Coauthors, 2011: Observations of Saharan dust microphysical and optical properties from the Eastern Atlantic during NAMMA airborne field campaign. *Atmospheric Chemistry and Physics*, **11 (2)**, 723–740, doi:10.5194/acp-11-723-2011.

Chen, J. L., T. Pekker, C. R. Wilson, B. D. Tapley, A. G. Kostianoy, J.-F. Cretaux, and E. S. Safarov, 2017: Long-term Caspian Sea level change. *Geophysical Research Letters*, **44 (13)**, 6993–7001, doi:10.1002/2017gl073958.

Creamean, J. M., A. B. White, P. Minnis, R. Palikonda, D. A. Spangenberg, and K. A. Prather, 2016: The relationships between insoluble precipitation residues, clouds, and precipitation over California's southern Sierra Nevada during winter storms. *Atmospheric Environment*, **140**, 298–310, doi:10.1016/j.atmosenv.2016.06.016.

Creamean, J. M., and Coauthors, 2013: Dust and biological aerosols from the Sahara and Asia influence precipitation in the Western U.S. *Science*, **339 (6127)**, 1572–1578, doi:10.1126/science.1227279.

DeMott, P. J., K. Sassen, M. R. Poellot, D. Baumgardner, D. C. Rogers, S. D. Brooks, A. J. Prenni, and S. M. Kreidenweis, 2003: African dust aerosols as atmospheric ice nuclei. *Geophysical Research Letters*, **30 (14)**, doi:10.1029/2003gl017410.

Dubovik, O., B. Holben, T. F. Eck, A. Smirnov, Y. J. Kaufman, M. D. King, D. Tanré, and I. Slutsker, 2002: Variability of absorption and optical properties of key aerosol types observed in worldwide locations. *Journal of the Atmospheric Sciences*, **59 (3)**, 590–608, doi:10.1175/1520-0469(2002)059⟨0590:voaaop⟩2.0.co;2.

Duce, R. A., C. K. Unni, B. J. Ray, J. M. Prospero, and J. T. Merrill, 1980: Long-range atmospheric transport of soil dust from Asia to the tropical North Pacific: Temporal variability. *Science*, **209 (4464)**, 1522–1524, doi:10.1126/science.209.4464.1522.

Dunion, J. P., and C. S. Velden, 2004: The impact of the Saharan Air Layer on Atlantic tropical cyclone activity. *Bulletin of the American Meteorological Society*, **85 (3)**, 353–366, doi:10.1175/bams-85-3-353.

Evan, A. T., J. Dunion, J. A. Foley, A. K. Heidinger, and C. S. Velden, 2006: New evidence for a relationship between Atlantic tropical cyclone activity and African dust outbreaks. *Geophysical Research Letters*, **33 (19)**, doi:10.1029/2006gl026408.

Evan, A. T., C. Flamant, S. Fiedler, and O. Doherty, 2014: An analysis of aeolian dust in climate models. *Geophysical Research Letters*, **41 (16)**, 5996–6001, doi:10.1002/2014gl060545.

Evan, A. T., and S. Mukhopadhyay, 2010: African dust over the Northern Tropical Atlantic: 1955–2008. *Journal of Applied Meteorology and Climatology*, **49 (11)**, 2213–2229, doi:10.1175/2010jamc2485.1.

Evan, A. T., D. J. Vimont, A. K. Heidinger, J. P. Kossin, and R. Bennartz, 2009: The role of aerosols in the evolution of tropical North Atlantic ocean temperature anomalies. *Science*, **324 (5928)**, 778–781, doi:10.1126/science.1167404.

Fan, J., and Coauthors, 2014: Aerosol impacts on California winter clouds and precipitation during CalWater 2011: local pollution versus long-range transported dust. *Atmospheric Chemistry and Physics*, **14 (1)**, 81–101, doi:10.5194/acp-14-81-2014.

Foltz, G. R., and M. J. McPhaden, 2008: Impact of Saharan Dust on Tropical North Atlantic SST. *Journal of Climate*, **21 (19)**, 5048–5060, doi:10.1175/2008jcli2232.1.

Formenti, P., 2003: Chemical composition of mineral dust aerosol during the Saharan Dust Experiment (SHADE) airborne campaign in the Cape Verde region, september 2000. *Journal of Geophysical Research*, **108 (D18)**, doi:10.1029/2002jd002648.

Formenti, P., and Coauthors, 2008: Regional variability of the composition of mineral dust from western Africa: Results from the AMMA SOP0/DABEX and DODO field campaigns. *Journal of Geophysical Research*, **113**, doi:10.1029/2008jd009903.

Foster, M. J., and A. Heidinger, 2013: PATMOS-x: Results from a diurnally corrected 30-yr satellite cloud climatology. *Journal of Climate*, **26 (2)**, 414–425, doi:10.1175/jcli-d-11-00666.1.

Ge, J. M., J. P. Huang, C. P. Xu, Y. L. Qi, and H. Y. Liu, 2014: Characteristics of Taklimakan dust emission and distribution: A satellite and reanalysis field perspective. *Journal of Geophysical Research: Atmospheres*, **119 (20)**, 11,772–11,783, doi:10.1002/2014jd022280.

Gelaro, R., and Coauthors, 2017: The Modern-Era Retrospective Analysis for Research and Applications, Version 2 (MERRA-2). *Journal of Climate*, **30 (14)**, 5419–5454, doi:10.1175/jcli-d-16-0758.1.

Giles, D. M., and Coauthors, 2012: An analysis of AERONET aerosol absorption properties and classifications representative of aerosol source regions. *Journal of Geophysical Research: Atmospheres*, **117 (D17)**, n/a–n/a, doi:10.1029/2012jd018127.

Gillette, D. A., I. H. Blifford, and D. W. Fryrear, 1974: The influence of wind velocity on the size distributions of aerosols generated by the wind erosion of soils. *Journal of Geophysical Research*, **79 (27)**, 4068–4075, doi:10.1029/jc079i027p04068.

Ginoux, P., J. M. Prospero, T. E. Gill, N. C. Hsu, and M. Zhao, 2012: Global-scale attribution of anthropogenic and natural dust sources and their emission rates based on MODIS Deep Blue aerosol products. *Reviews of Geophysics*, **50 (3)**, doi:10.1029/2012rg000388.

Griffin, D. W., 2007: Atmospheric movement of microorganisms in clouds of desert dust and implications for human health. *Clinical Microbiology Reviews*, **20 (3)**, 459–477, doi:10.1128/cmr.00039-06.

Hand, J. L., W. H. White, K. A. Gebhart, N. P. Hyslop, T. E. Gill, and B. A. Schichtel, 2016: Earlier onset of the spring fine dust season in the southwestern United States. *Geophysical Research Letters*, **43 (8)**, 4001–4009, doi:10.1002/2016gl068519.

Heidinger, A. K., M. J. Foster, A. Walther, and X. T. Zhao, 2014: The Pathfinder Atmospheres–Extended AVHRR climate dataset. *Bulletin of the American Meteorological Society*, **95 (6)**, 909–922, doi:10.1175/bams-d-12-00246.1.

Holben, B., and Coauthors, 1998: AERONET—a federated instrument network and data archive for aerosol characterization. *Remote*

*Sensing of Environment*, **66 (1)**, 1–16, doi:10.1016/s0034-4257(98)00031-5.

Hsu, N. C., R. Gautam, A. M. Sayer, C. Bettenhausen, C. Li, M. J. Jeong, S.-C. Tsay, and B. N. Holben, 2012: Global and regional trends of aerosol optical depth over land and ocean using SeaWiFS measurements from 1997 to 2010. *Atmospheric Chemistry and Physics*, **12 (17)**, 8037–8053, doi:10.5194/acp-12-8037-2012.

Hsu, N. C., M.-J. Jeong, C. Bettenhausen, A. M. Sayer, R. Hansell, C. S. Seftor, J. Huang, and S.-C. Tsay, 2013: Enhanced deep blue aerosol retrieval algorithm: The second generation. *Journal of Geophysical Research: Atmospheres*, **118 (16)**, 9296–9315, doi:10.1002/jgrd.50712.

Hsu, N. C., A. M. Sayer, C. Bettenhausen, J. Lee, R. C. Levy, S. Mattoo, L. A. Munchak, and R. Kleidman, 2014: Comparing MODIS C6 'Deep Blue' and 'Dark Target' aerosol data. Tech. rep., NASA.

Ichoku, C., 2005: Quantitative evaluation and intercomparison of morning and afternoon Moderate Resolution Imaging Spectroradiometer (MODIS) aerosol measurements from Terra and Aqua. *Journal of Geophysical Research*, **110 (D10)**, doi:10.1029/2004jd004987.

Isono, K., M. Kombayasi, and A. Ono, 1959: The nature and origin of ice nuclei in the atmosphere. *J. Meteorol. Soc. Japan*, **37**, 211–233.

Izhitskiy, A. S., and Coauthors, 2016: Present state of the Aral Sea: diverging physical and biological characteristics of the residual basins. *Scientific Reports*, **6 (1)**, doi:10.1038/srep23906.

Kahn, R. A., M. J. Garay, D. L. Nelson, K. K. Yau, M. A. Bull, B. J. Gaitley, J. V. Martonchik, and R. C. Levy, 2007: Satellite-derived aerosol optical depth over dark water from MISR and MODIS: Comparisons with AERONET and implications for climatological studies. *Journal of Geophysical Research*, **112 (D18)**, doi:10.1029/2006jd008175.

Kaufman, Y. J., 2005: Dust transport and deposition observed from the Terra-Moderate Resolution Imaging Spectroradiometer (MODIS) spacecraft over the Atlantic Ocean. *Journal of Geophysical Research*, **110 (D10)**, doi:10.1029/2003jd004436.

Kaufman, Y. J., I. Koren, L. A. Remer, D. Rosenfeld, and Y. Rudich, 2005: The effect of smoke, dust, and pollution aerosol on shallow cloud development over the Atlantic Ocean. *Proceedings of the National Academy of Sciences*, **102 (32)**, 11 207–11 212, doi:10.1073/pnas.0505191102.

Kaufman, Y. J., D. Tanré, L. A. Remer, E. F. Vermote, A. Chu, and B. N. Holben, 1997: Operational remote sensing of tropospheric aerosol over land from EOS moderate resolution imaging spectroradiometer. *Journal of Geophysical Research: Atmospheres*, **102 (D14)**, 17 051–17 067, doi:10.1029/96jd03988.

Klaver, A., and Coauthors, 2011: Physico-chemical and optical properties of Sahelian and Saharan mineral dust: in situ measurements during the GERBILS campaign. *Quarterly Journal of the Royal Meteorological Society*, **137 (658)**, 1193–1210, doi:10.1002/qj.889.

Kleidman, R. G., N. T. O'Neill, L. A. Remer, Y. J. Kaufman, T. F. Eck, D. Tanré, O. Dubovik, and B. N. Holben, 2005: Comparison of Moderate Resolution Imaging Spectroradiometer (MODIS) and Aerosol Robotic Network (AERONET) remote-sensing retrievals of aerosol fine mode fraction over ocean. *Journal of Geophysical Research*, **110 (D22)**, doi:10.1029/2005jd005760.

Kleidman, R. G., A. Smirnov, R. C. Levy, S. Mattoo, and D. Tanre, 2012: Evaluation and wind speed dependence of MODIS aerosol retrievals over open ocean. *IEEE Transactions on Geoscience and Remote Sensing*, **50 (2)**, 429–435, doi:10.1109/tgrs.2011.2162073.

Lehahn, Y., I. Koren, E. Boss, Y. Ben-Ami, and O. Altaratz, 2010: Estimating the maritime component of aerosol optical depth and its dependency on surface wind speed using satellite data. *Atmospheric Chemistry and Physics*, **10 (14)**, 6711–6720, doi:10.5194/acp-10-6711-2010.

Lynn, B. H., and Coauthors, 2016: The sensitivity of hurricane Irene to aerosols and ocean coupling: Simulations with WRF spectral bin microphysics. *Journal of the Atmospheric Sciences*, **73 (2)**, 467–486, doi:10.1175/jas-d-14-0150.1.

Mahowald, N. M., and C. Luo, 2003: A less dusty future? *Geophysical Research Letters*, **30 (17)**, n/a–n/a, doi:10.1029/2003gl017880.

Malm, W. C., J. F. Sisler, D. Huffman, R. A. Eldred, and T. A. Cahill, 1994: Spatial and seasonal trends in particle concentration and optical extinction in the United States. *Journal of Geophysical Research*, **99 (D1)**, 1347, doi:10.1029/93jd02916.

Mani, M., and R. Pillai, 2010: Impact of dust on solar photovoltaic (PV) performance: Research status, challenges and recommendations. *Renewable and Sustainable Energy Reviews*, **14 (9)**, 3124–3131, doi:10.1016/j.rser.2010.07.065.

Miller, R. L., and I. Tegen, 1998: Climate response to soil dust aerosols. *Journal of Climate*, **11 (12)**, 3247–3267, doi:10.1175/1520-0442(1998)011⟨3247:crtsda⟩2.0.co;2.

Norris, J. R., and A. T. Evan, 2015: Empirical removal of artifacts from the ISCCP and PATMOS-x satellite cloud records. *Journal of Atmospheric and Oceanic Technology*, **32 (4)**, 691–702, doi:10.1175/jtech-d-14-00058.1.

O'Neill, N. T., 2003: Spectral discrimination of coarse and fine mode optical depth. *Journal of Geophysical Research*, **108 (D17)**, doi:10.1029/2002jd002975.

Pandey, S. K., V. Vinoj, K. Landu, and S. S. Babu, 2017: Declining pre-monsoon dust loading over South Asia: Signature of a changing regional climate. *Scientific Reports*, **7 (1)**, doi:10.1038/s41598-017-16338-w.

Prospero, J. M., 1999: Long-range transport of mineral dust in the global atmosphere: Impact of African dust on the environment of the southeastern United States. *Proceedings of the National Academy of Sciences*, **96 (7)**, 3396–3403, doi:10.1073/pnas.96.7.3396.

Prospero, J. M., and O. L. Mayol-Bracero, 2013: Understanding the transport and impact of African dust on the Caribbean Basin. *Bulletin of the American Meteorological Society*, **94 (9)**, 1329–1337, doi:10.1175/bams-d-12-00142.1.

Prospero, J. M., and R. T. Nees, 1986: Impact of the North African drought and El Niño on mineral dust in the Barbados trade winds. *Nature*, **320 (6064)**, 735–738, doi:10.1038/320735a0.

Prospero, J. M., and Coauthors, 1996: Atmospheric deposition of nutrients to the North Atlantic Basin. *Nitrogen Cycling in the North Atlantic Ocean and its Watersheds*, Springer Netherlands, 27–73, doi:10.1007/978-94-009-1776-7_2.

Pu, B., and P. Ginoux, 2017: Projection of American dustiness in the late 21st century due to climate change. *Scientific Reports*, **7 (1)**, doi:10.1038/s41598-017-05431-9.

Qian, W., L. Quan, and S. Shi, 2002: Variations of the dust storm in China and its climatic control. *Journal of Climate*, **15 (10)**, 1216–1229, doi:10.1175/1520-0442(2002)015⟨1216:votdsi⟩2.0.co;2.

Ralph, F. M., and Coauthors, 2016: CalWater field studies designed to quantify the roles of atmospheric rivers and aerosols in modulating U.S. West Coast precipitation in a changing climate. *Bulletin of the American Meteorological Society*, **97 (7)**, 1209–1228, doi:10.1175/bams-d-14-00043.1.

Randles, C. A., and Coauthors, 2017: The MERRA-2 aerosol reanalysis, 1980 onward. Part I: System description and data assimilation evaluation. *Journal of Climate*, **30 (17)**, 6823–6850, doi:10.1175/jcli-d-16-0609.1.

Remer, L. A., S. Mattoo, R. C. Levy, A. Heidinger, R. B. Pierce, and M. Chin, 2012: Retrieving aerosol in a cloudy environment: aerosol product availability as a function of spatial resolution. *Atmospheric Measurement Techniques*, **5 (7)**, 1823–1840, doi:10.5194/amt-5-1823-2012.

Remer, L. A., and Coauthors, 2005: The MODIS aerosol algorithm, products, and validation. *Journal of the Atmospheric Sciences*, **62 (4)**, 947–973, doi:10.1175/jas3385.1.

Remer, L. A., and Coauthors, 2008: Global aerosol climatology from the MODIS satellite sensors. *Journal of Geophysical Research*, **113 (D14)**, doi:10.1029/2007jd009661.

Ridley, D. A., C. L. Heald, J. F. Kok, and C. Zhao, 2016: An observationally constrained estimate of global dust aerosol optical depth. *Atmospheric Chemistry and Physics*, **16 (23)**, 15 097–15 117, doi:10.5194/acp-16-15097-2016.

Rosenfeld, D., Y. Rudich, and R. Lahav, 2001: Desert dust suppressing precipitation: A possible desertification feedback loop. *Proceedings of the National Academy of Sciences*, **98 (11)**, 5975–5980, doi:10.1073/pnas.101122798.

Ryder, C. L., and Coauthors, 2013: Optical properties of Saharan dust aerosol and contribution from the coarse mode as measured during the Fennec 2011 aircraft campaign. *Atmospheric Chemistry and Physics*, **13 (1)**, 303–325, doi:10.5194/acp-13-303-2013.

Satheesh, S. K., J. Srinivasan, and K. K. Moorthy, 2006: Contribution of sea-salt to aerosol optical depth over the Arabian Sea derived from MODIS observations. *Geophysical Research Letters*, **33 (3)**, doi:10.1029/2005gl024856.

Sato, M., J. E. Hansen, M. P. McCormick, and J. B. Pollack, 1993: Stratospheric aerosol optical depths, 1850–1990. *Journal of Geophysical Research*, **98 (D12)**, 22 987, doi:10.1029/93jd02553.

Sayer, A. M., N. C. Hsu, C. Bettenhausen, and M.-J. Jeong, 2013: Validation and uncertainty estimates for MODIS collection 6 "Deep Blue" aerosol data. *Journal of Geophysical Research: Atmospheres*, **118 (14)**, 7864–7872, doi:10.1002/jgrd.50600.

Shao, Y., 2008: *Physics and Modeling of Wind Erosion*. Springer Science and Business Media.

Shao, Y., M. R. Raupach, and P. A. Findlater, 1993: Effect of saltation bombardment on the entrainment of dust by wind. *Journal of Geophysical Research*, **98 (D7)**, 12 719, doi:10.1029/93jd00396.

Smirnov, A., B. N. Holben, T. F. Eck, O. Dubovik, and I. Slutsker, 2003: Effect of wind speed on columnar aerosol optical properties at Midway Island. *Journal of Geophysical Research: Atmospheres*, **108 (D24)**, n/a–n/a, doi:10.1029/2003jd003879.

Stith, J. L., and Coauthors, 2009: An overview of aircraft observations from the Pacific Dust Experiment campaign. *Journal of Geophysical Research*, **114 (D5)**, doi:10.1029/2008jd010924.

Sun, J., M. Zhang, and T. Liu, 2001: Spatial and temporal characteristics of dust storms in China and its surrounding regions, 1960-1999: Relations to source area and climate. *Journal of Geophysical Research: Atmospheres*, **106 (D10)**, 10 325–10 333, doi:10.1029/2000jd900665.

Tanré, D., Y. J. Kaufman, M. Herman, and S. Mattoo, 1997: Remote sensing of aerosol properties over oceans using the MODIS/EOS spectral radiances. *Journal of Geophysical Research: Atmospheres*, **102 (D14)**, 16 971–16 988, doi:10.1029/96jd03437.

Tegen, I., M. Werner, S. P. Harrison, and K. E. Kohfeld, 2004: Relative importance of climate and land use in determining present and future global soil dust emission. *Geophysical Research Letters*, **31 (5)**, n/a–n/a, doi:10.1029/2003gl019216.

Textor, C., and Coauthors, 2006: Analysis and quantification of the diversities of aerosol life cycles within AeroCom. *Atmospheric Chemistry and Physics*, **6 (7)**, 1777–1813, doi:10.5194/acp-6-1777-2006.

Tong, D. Q., J. X. L. Wang, T. E. Gill, H. Lei, and B. Wang, 2017: Intensified dust storm activity and valley fever infection in the southwestern United States. *Geophysical Research Letters*, **44 (9)**, 4304–4312, doi:10.1002/2017gl073524.

Toth, T. D., and Coauthors, 2013: Investigating enhanced Aqua MODIS aerosol optical depth retrievals over the mid-to-high latitude Southern Oceans through intercomparison with co-located CALIOP, MAN, and AERONET data sets. *Journal of Geophysical Research: Atmospheres*, **118 (10)**, 4700–4714, doi:10.1002/jgrd.50311.

Twomey, S., 1977: The influence of pollution on the shortwave albedo of clouds. *Journal of the Atmospheric Sciences*, **34 (7)**, 1149–1152, doi:10.1175/1520-0469(1977)034⟨1149:tiopot⟩2.0.co;2.

Uematsu, M., R. A. Duce, J. M. Prospero, L. Chen, J. T. Merrill, and R. L. McDonald, 1983: Transport of mineral aerosol from Asia over the North Pacific ocean. *Journal of Geophysical Research: Oceans*, **88 (C9)**, 5343–5352, doi:10.1029/jc088ic09p05343.

Yoshioka, M., N. M. Mahowald, A. J. Conley, W. D. Collins, D. W. Fillmore, C. S. Zender, and D. B. Coleman, 2007: Impact of desert dust radiative forcing on sahel precipitation: Relative importance of dust compared to sea surface temperature variations, vegetation changes, and greenhouse gas warming. *Journal of Climate*, **20 (8)**, 1445–1467, doi:10.1175/jcli4056.1.

Yumimoto, K., K. Eguchi, I. Uno, T. Takemura, Z. Liu, A. Shimizu, N. Sugimoto, and K. Strawbridge, 2010: Summertime trans-pacific transport of asian dust. *Geophysical Research Letters*, **37 (18)**, n/a–n/a, doi:10.1029/2010gl043995.

Zhao, T. X.-P., I. Laszlo, W. Guo, A. Heidinger, C. Cao, A. Jelenak, D. Tarpley, and J. Sullivan, 2008: Study of long-term trend in aerosol optical thickness observed from operational AVHRR satellite instrument. *Journal of Geophysical Research*, **113 (D7)**, doi:10.1029/2007jd009061.

Zhao, T. X.-P., L. L. Stowe, A. Smirnov, D. Crosby, J. Sapper, and C. R. McClain, 2002: Development of a global validation package for satellite oceanic aerosol optical thickness retrieval based on AERONET observations and its application to NOAA/NESDIS operational aerosol retrievals. *Journal of the Atmospheric Sciences*, **59 (3)**, 294–312, doi:10.1175/1520-0469(2002)059⟨0294:doagvp⟩2.0.co;2.

Zhao, X., and N. C. Program, 2017: Noaa climate data record (cdr) of avhrr daily and monthly aerosol optical thickness (aot) over global oceans, version 3.0. *NOAA National Centers for Environmental Information*, doi:10.7289/V5SB43PD.